NANO LETTERS

2008
Vol. 8, No. 10
3238-3243

Efficient Low-Temperature Thermophotovoltaic Emitters from Metallic Photonic Crystals

Prashant Nagpal,† Sang Eon Han,† Andreas Stein,‡ and David J. Norris*,†

Department of Chemical Engineering and Materials Science, University of Minnesota, 421 Washington Avenue SE, Minneapolis, Minnesota 55455, and Department of Chemistry, University of Minnesota, 207 Pleasant Street SE, Minneapolis, Minnesota 55455

Received June 2, 2008; Revised Manuscript Received August 18, 2008

ABSTRACT

We examine the use of metallic photonic crystals as thermophotovoltaic emitters. We coat silica woodpile structures, created using direct laser writing, with tungsten or molybdenum. Optical reflectivity and thermal emission measurements near 650 °C demonstrate that the resulting structures should provide efficient emitters at relatively low temperatures. When matched to InGaAsSb photocells, our structures should generate over ten times more power than solid emitters while having an optical-to-electrical conversion efficiency above 32%. At such low temperatures, these emitters have promise not only in solar energy but also in harnessing geothermal and industrial waste heat.

A fundamental difficulty in the efficient generation of electricity from sunlight is the energetically broad distribution of solar photons. Because standard photovoltaic devices transform photons into essentially isoenergetic electrons, and each photon typically creates at most one electron, energy mismatches between photons and electrons lead to waste. While many approaches[1−3] aim to improve this direct photon-to-electron conversion, a less-studied alternative is to transform sunlight first into low-energy photons.[4−6] A material, heated by the sun, can then thermally re-emit infrared light into a well-matched conventional photocell. In principle, this thermophotovoltaic (TPV) process can be very efficient, but it has been limited by the thermal emission spectra of real materials. Ideally, the emitting material would convert all absorbed energy into a narrow band of thermal emission that is tailored to an available narrow-bandgap semiconductor photocell. If instead the emission spectrum is too broad, too weak, or poorly matched to the photocell response, inefficiency is introduced.[4−6]

While several materials have been considered for improved TPV emitters,[5] three-dimensionally structured solids known as photonic crystals[7] can provide new possibilities.[8] Their thermal emission can be tailored by prohibiting thermal emission in certain energy ranges.[9−16] Instead of a broad blackbody-like spectrum, proper design can lead to a narrow and intense emission peak. To examine this phenomenon, the "woodpile" photonic crystal structure (Figure 1a) has been studied. Indeed, theory and experiments have demonstrated its ability to modify the thermal emission spectrum.[8,10,14] However, the possibility that this structure could yield efficient TPV emitters has not been fully explored. For example, it is unclear whether photonic crystals could actually survive the elevated temperatures previously considered necessary for TPV applications.[17] Even when they are made from refractory metals that have high melting temperatures, grain growth can destroy the intricate microstructure in the photonic crystal. To complicate matters, further study has been impeded due to the complex and expensive process required to obtain these materials.[10]

Here, we fabricate and examine the properties of metallic woodpile structures for use as TPV emitters. We consider relatively low temperatures (near 650 °C), where the structures are known to be stable. In this case, we show that optical-to-electrical conversion efficiencies above 30% can be expected. Therefore, these results confirm the great potential of these materials for TPV applications. Further, at such low temperatures these emitters have promise not only for solar energy conversion but also for harnessing heat from geothermal and industrial sources.

To address the fabrication challenge, we employ an extremely simple technique known as direct laser writing (DLW).[18−23] This approach typically moves the focused spot of an infrared laser through a thin film of organic photoresist to form lines by multiphoton polymerization. Proper layering of such lines can lead to a scaffold with the woodpile

* Corresponding author. E-mail: dnorris@umn.edu.
† Department of Chemical Engineering and Materials Science.
‡ Department of Chemistry.

10.1021/nl801571z CCC: $40.75 © 2008 American Chemical Society
Published on Web 09/10/2008

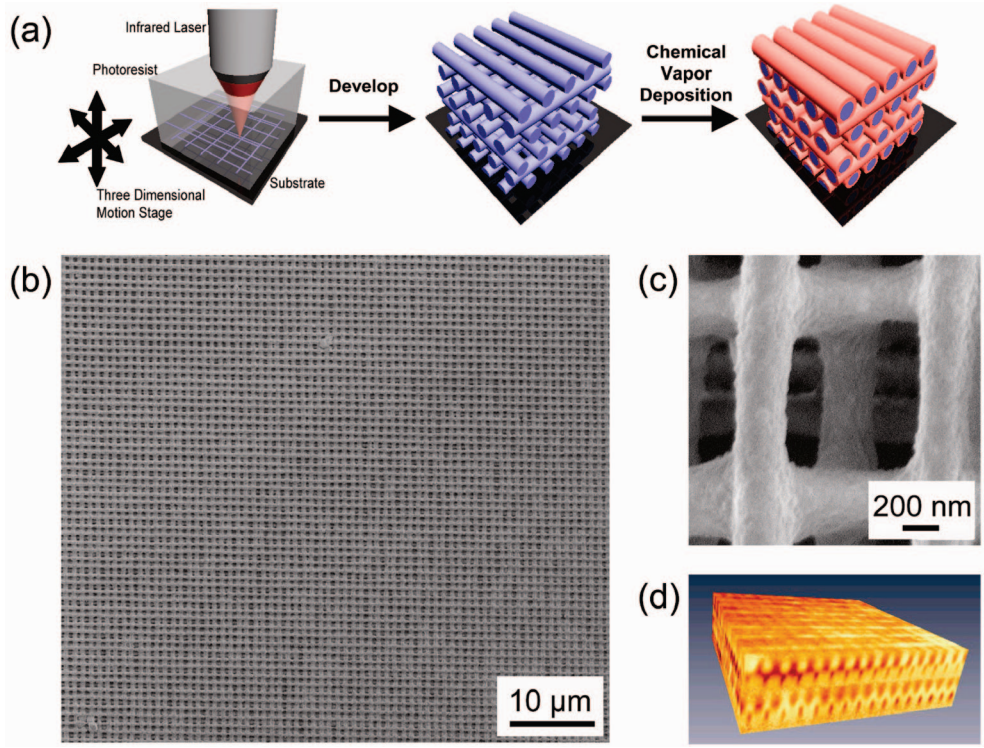

Figure 1. (a) To fabricate metallic photonic crystals with direct laser writing, a confocal microscope defines the woodpile structure in a film of methylsilsesquioxane-based photoresist. After development, the structure is coated with tungsten or molybdenum using chemical vapor deposition. (b) Electron micrograph of the top view of an 8-layer woodpile scaffold before metallization (900 nm line spacing). If this scaffold was coated with metal, its thermal emission could in principle be matched to a silicon photocell. (c) Detailed view of the sample in (b) tilted to show the structure down to the lowest layer. (d) Three-dimensional reconstruction from confocal optical micrographs obtained for a woodpile with a 1.8 μm line spacing. If coated with metal, the thermal emission from this structure could be matched to an InGaAsSb photocell. The interlayer spacing in the z-direction (perpendicular to the substrate) is 0.4 μm.

structure. For thermal emission, this structure could then be coated with a refractory metal. Unfortunately, because organic photoresists do not have high thermal stability, these scaffolds cannot survive typical coating processes, such as chemical vapor deposition (CVD). Moreover, even if gentler deposition schemes are employed,[24,25] the organic material typically remains in the scaffold, severely limiting its temperature range. Consequently, thermal emitters have not yet been demonstrated using DLW.

We overcome these problems by utilizing a recently developed methylsilsesquioxane-based photoresist that allows high temperature processing.[26,27] After laser exposure, the resist was developed and heated in an inert atmosphere to convert the structure into silica, thereby making it thermally robust. The resultant scaffold was then coated with a shell of tungsten (W) or molybdenum (Mo) of desired thickness with a simple home-built CVD reactor. (Details are described in the Supporting Information.) The total process is depicted in Figure 1a.

DLW allows the lattice parameters of the woodpile, which control the thermal emission spectrum, to be varied easily. While we concentrate our analysis below on 8-layer structures fabricated to produce thermal emission well matched to the electronic bandgap (0.53 eV) of InGaAsSb photocells,[28,29] we also present woodpiles appropriate for silicon photocells. W and Mo were chosen as metals because they have extremely low vapor pressures at the temperatures necessary for TPV devices. Another factor is their shallow skin depths. For example, at a wavelength of 1.77 μm (0.7 eV), W has a skin depth of 46 nm and the transmission through a 100 nm thick film is only 0.4%. Thus, after coating the scaffold with films of such thickness, the silica core can remain in the structure without playing a role in the thermal emission. Calculations show that the coated woodpiles behave as if they contained solid rods of metal.

Figure 1b,c shows the excellent fidelity of the top surface of our silica scaffolds before metallization. To examine their three-dimensional (3D) structure, we also infiltrated them with fluorescent dye and collected internal images with laser-scanning confocal microscopy. A 3D reconstruction obtained from a series of such images is shown in Figure 1d. For CVD, tungsten hexacarbonyl or molybdenum hexacarbonyl were used as molecular precursors.[30] Figure 2, panels a and b−d, represents typical W- and Mo-coated woodpiles, respectively. (Additional samples are shown in Figure S1 in the Supporting Information.) X-ray microdiffractometry data (Figure S2 in the Supporting Information) confirm that the coatings were metallic W and Mo. Thinner coatings (50−100 nm) could be obtained with nitrogen as the carrier gas (Figure 2a) and thicker coatings (100−300 nm) with mixtures of nitrogen and hydrogen (Figure 2b) under otherwise identical CVD conditions.[30] The amount of added precursor also influenced this thickness.

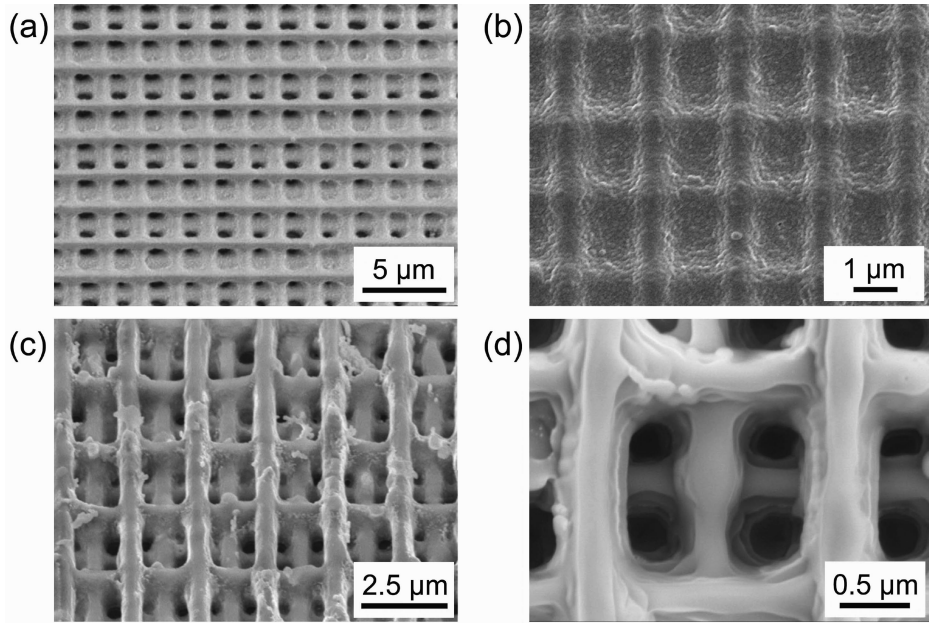

Figure 2. (a) Electron micrograph of the top view of an 8-layer silica woodpile with a 100 nm thick tungsten coating. (b) Another 8-layer sample with nearly complete infiltration with molybdenum. (c) Eight-layer silica woodpile with a 100 nm molybdenum coating after heating for two hours at 650 °C. (d) A higher magnification image of the sample shown in panel c obtained at an electron acceleration voltage of 6 kV to reveal the silica rods under the molybdenum coating.

We then analyzed these structures both structurally and optically for thermal emission. First, they were heated under inert atmosphere at 650 °C for two hours. Figure 2c shows a Mo woodpile after this treatment. (Heat-treated silica scaffolds are also shown in Figure S1 in the Supporting Information.) The SiO_2−Mo core−shell structure remains, as revealed in micrographs obtained at high electron acceleration voltages (Figure 2d). More importantly, no metal grain growth was observed due to heating. (The small metal flakes on the top surfaces of our samples were present prior to the heat treatment as seen in Figure S1 in the Supporting Information. They were deposited due to the simplicity of our CVD apparatus.) Second, we measured the reflectivity, R, of the samples using a home-built Fourier-transform infrared (FTIR) microscope.[31] Data from InGaAs and InSb detectors were combined to cover the wavelength range relevant for our thermal emission experiments. Figure 3a,b shows R versus wavelength for Mo and W woodpiles. Because of the low transmission of our structures, their absorptivity should be approximately $1 - R$. To test this, we also compare the measured $1 - R$ with the absorptivity calculated for plane waves incident normal to the structure surface using the transfer matrix method combined with multiple scattering (Figure 3a,b).[32] While a detailed fit was not possible due to the time required for electromagnetic calculations involving thin metals, qualitative agreement was achieved using parameters estimated from experimental micrographs. For both Mo and W, the experimental curves were smoother than the theoretical predictions, most likely due to disorder, but the absorptivity and the experimental $1 - R$ are quite similar at longer wavelengths. At shorter wavelengths (less than 1.75 and 2.0 μm for Mo and W, respectively), a sudden drop in the calculated absorptivity is absent from the experimental $1 - R$. This is caused by higher order reflections that direct light outside the collection cone of our microscope objective. Thus, the use of the measured $1 - R$ to approximate absorptivity will be strictly valid only at longer wavelengths.

Absorptivity is a critical parameter because at thermal equilibrium Kirchhoff's law states that it is equivalent to emissivity, from which the thermal emission intensity can be determined. Assuming low transmissivity, the emissivity for our samples will approach unity (the ideal blackbody limit) for wavelengths where the extracted absorptivity is high and will approach zero where the extracted absorptivity is low. Consequently, Figure 3a,b demonstrates two key advantages of our photonic crystals for tailoring thermal emission. First, due to the existence of a metallicity gap,[10] light is not allowed to propagate inside these structures for wavelengths longer than 2.5 μm. This leads to low absorptivity and, hence, weak emissivity above this wavelength. (This is also consistent with the high reflectivity measured for our samples from 2.5 to 15 μm on a low-resolution commercial FTIR microscope.) Second, due to the slow optical group velocity that occurs near the edge of the metallicity gap, light-matter interactions should be enhanced when compared to a solid film of the same metal. This leads to higher absorptivity and, hence, higher emissivity near 2 and 2.2 μm for Mo and W, respectively (see Figure S3 in the Supporting Information). Therefore, the emissivity of our W and Mo woodpiles can be tailored to approach the blackbody limit at wavelengths in the vicinity of 2 μm, while decreasing to zero at longer wavelengths.

The measured thermal emission spectrum for a given temperature should then be the product of the extracted emissivity and the blackbody spectrum. We test this for the Mo woodpile in Figure 3c. We assume that the measured $1 - R$ (blue curve) is the emissivity. However, unlike an

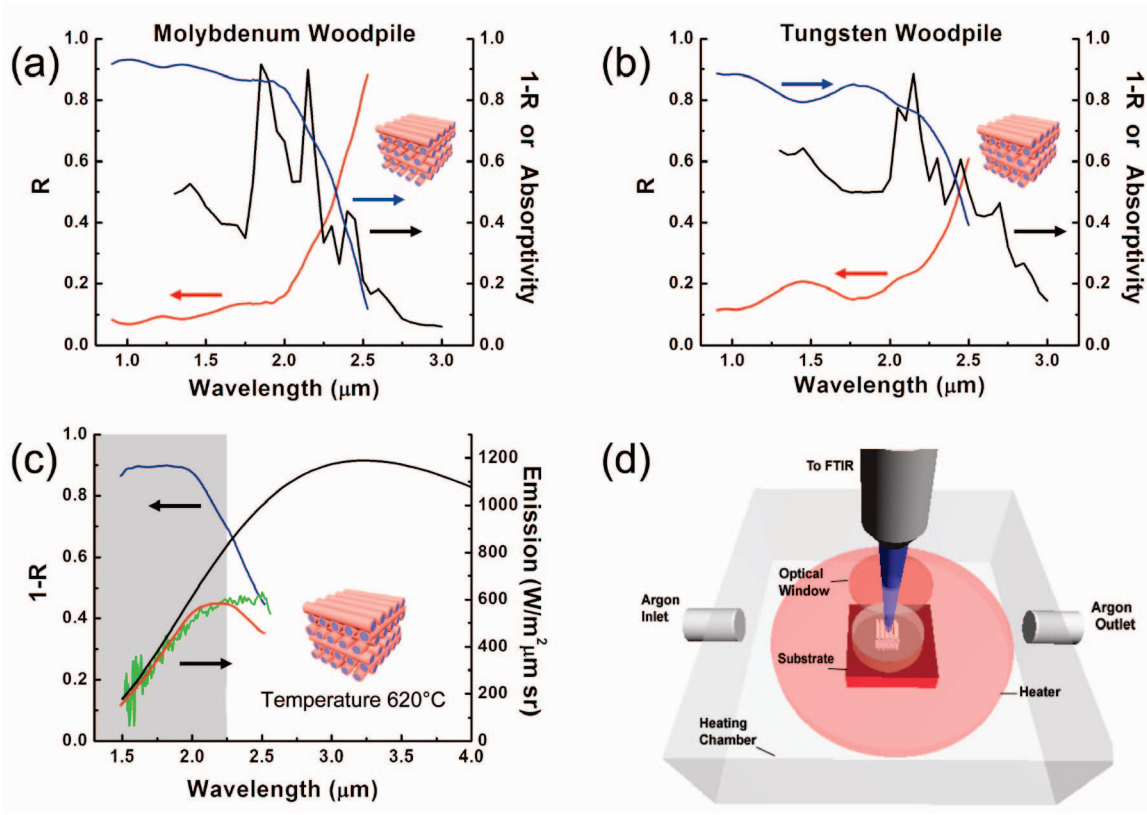

Figure 3. The measured optical reflectivity R (red curve) and $1 - R$ (blue curve) vs wavelength for (a) an 8-layer molybdenum woodpile (1.75 μm line spacing, 0.4 μm interlayer spacing, and 100 nm shell thickness) and (b) an 8-layer tungsten woodpile (2.0 μm line spacing, 0.6 μm interlayer spacing, and 140 nm shell thickness). The calculated absorptivity is also shown in both for comparison (black curves). (c) The measured $1 - R$ (blue curve) vs wavelength for a molybdenum woodpile (2.0 μm line spacing, 0.6 μm interlayer spacing, and 100 nm shell thickness). The expected thermal emission spectrum per unit solid angle at 620 °C (red curve), which is the product of the emissivity (approximated as the blue curve), and the calculated blackbody spectrum (black curve) at 620 °C is compared with the measured thermal emission spectrum per unit solid angle averaged over the collection angle of the microscope (green curve). The gray shaded area denotes the wavelength range in which InGaAsSb photocells can have an external quantum efficiency above 50% (ref 28). (d) The experimental setup used for the measurement of thermal emission spectra.

ideal blackbody, the photonic crystal will exhibit an emissivity that is directional. Thus, the experimental value represents an emissivity averaged over the finite solid angle collected by the microscope (0.67 sr around the surface normal). By multiplying this emissivity with the calculated blackbody spectrum per unit solid angle at 620 °C (black curve), we obtain the expected thermal emission spectrum per unit solid angle near normal for this temperature (red curve). To measure the actual emission spectrum, we used the apparatus shown in Figure 3d. An enclosed heating stage was mounted on the microscope to control the sample temperature under slowly flowing argon. A small orifice allowed emission from the sample surface to be collected by the microscope. The output was then directed toward a FTIR spectrometer and carefully calibrated with a lamp of known intensity. The measured thermal emission spectrum for 620 °C is shown in Figure 3c (green curve) up to the wavelength limit of our apparatus (2.5 μm). This spectrum agrees well with the predicted values, confirming that the samples behave as expected and that the emissivity extracted from our reflectivity data can be used to predict their thermal emission.

Such an emission spectrum is ideal for use as a low-temperature emitter for TPV conversion when it is coupled to an InGaAsSb photocell.[28,29] The gray region in Figure 3c denotes the wavelength range where the external quantum efficiency of this photocell can be above 50%. The emitted power density for our sample is close to the blackbody limit at wavelengths shorter than 2 μm where the response of the photocell is maximized, but decreases as the photocell response goes to zero at the bandgap of the semiconductor (0.53 eV or 2.34 μm). Thus, the emitted power can be utilized efficiently.

To quantify this further, we used the experimental emissivity spectrum extracted for the Mo woodpile in Figure 3a to determine several parameters relevant for TPV devices as a function of temperature. This emissivity represents an average over a solid angle of 1.26 sr around the surface normal. Beyond the long wavelength limit of the data, we used calculated values to extend the emissivity spectrum. In Figure 4a, the total radiated power per steradian for our woodpile (red curve) is compared to that of a blackbody (black curve) and a solid Mo film (blue curve). Due to the low emissivity of the woodpile at long wavelengths, its total radiated power is below that of the blackbody. However, because this radiated power is better matched to the photocell, the radiated-to-electrical power conversion efficiency can be much higher. Figure 4b shows this efficiency, assuming every

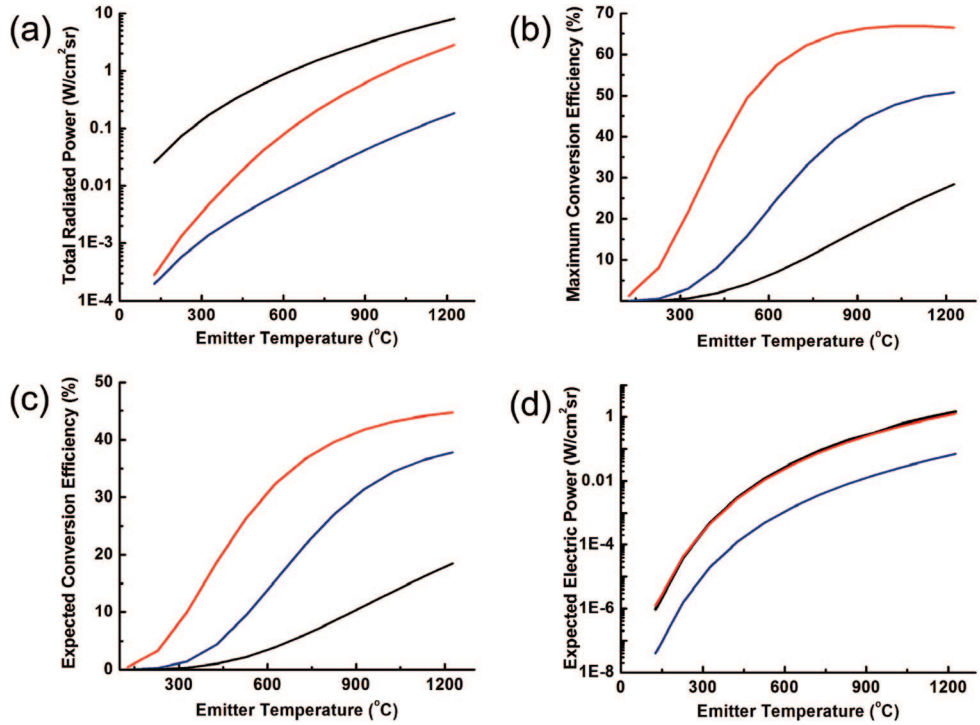

Figure 4. Using the data from Figure 3a, the temperature dependence of several parameters relevant for thermophotovoltaic devices were calculated. (a) The total radiated power per unit solid angle. (b) The maximum radiated-to-electrical conversion efficiency, assuming an InGaAsSb photocell with an external quantum efficiency of 100%. (c) The expected radiated-to-electrical conversion efficiency, using the published external quantum efficiencies for an InGaAsSb photocell (ref 28). (d) The expected electric power, which is the product of the curves in panels a and c. For each plot, the molybdenum woodpile (red curve) is compared with a blackbody (black curve) and a solid molybdenum film (blue curve).

emitted photon with energy above the InGaAsSb bandgap is converted to an electron with 0.53 eV. This represents an ideal InGaAsSb photocell with an external quantum efficiency of 100% but still includes inefficiencies due to photon-electron energy mismatches. In Figure 4c, we plot the efficiency using the measured external quantum efficiencies for real InGaAsSb photocells.[28] In both plots, the woodpile exhibits greatly improved conversion efficiency compared to the blackbody and solid film, especially at low temperatures. For example, at 650 °C the expected conversion efficiency for the woodpile using a real photocell (Figure 4c) is 32%, compared to 17 and 4% for the solid film and blackbody, respectively.

It is perhaps surprising that the solid film would also provide reasonable efficiencies. This occurs because solid Mo has low emissivity at long wavelengths and consequently, the power radiated at wavelengths that cannot be converted by the photocell is reduced. However, the weakness of the solid film is that it also has lower emissivity at useful wavelengths. If we multiply the total radiated power per steradian (Figure 4a) by the expected conversion efficiency (Figure 4c) to calculate the expected electrical power (Figure 4d), we find that the Mo woodpile at 45 mW/cm^2/sr is able to produce over an order of magnitude more power than the solid film. Although the blackbody generates the most electrical power, the woodpile is comparable. This is expected because the emission of our photonic crystal at useful wavelengths does not exceed that of the blackbody. But, because the woodpile generates this power much more efficiently, the heat required to maintain the temperature of the emitter would be decreased. For example, in solar thermophotovoltaics a smaller solar collector would be necessary to heat the emitter, decreasing cost and complexity. Therefore, due to the ability of the photonic crystal to tailor the emissivity of the metal, the best combination of generated power and efficiency can be obtained.

The above values were achieved at a relatively low temperature of 650 °C. At this temperature, we know that our structures can survive. Prior work had suggested to operate photonic crystal emitters above 1000 °C.[8] Clearly, at higher temperatures the total radiated power (Figure 4a) and, hence, the generated electrical power (Figure 4d) would increase. However, at such temperatures grain growth would destroy the microstructure.[17] Consequently, we have compromised on the electrical power per unit area while still maintaining high efficiency to obtain a structure that is useful at realistic operational temperatures. In addition, low temperature operation may allow applications beyond solar energy, such as conversion of waste heat from industrial sources.

So far our analysis has avoided the complicated experimental and theoretical issue of the angle dependence of the emission. Preliminary calculations show that the emissivity of metal woodpiles decreases for directions far from the surface normal, as expected for any nonideal surface due to increased reflectivity at glancing angles. Thus, the total power radiated into 2π sr by the woodpile will be lower, when compared to the blackbody, than Figure 4a implies. The

relative electrical power (Figure 4d) will also be lower. However, because the thermal emission from the photonic crystal will be more directional, it may in fact provide more efficient collection by the photocell, providing another advantage.

The performance of our photonic crystal emitters could be improved further in several ways. First, we could utilize standard techniques in thermophotovoltaic devices, such as incorporating reflectors, which recycle long-wavelength emitted photons back to the photonic crystal to help maintain its temperature.[1,16] Second, we could optimize the structure of the photonic crystal to improve the thermal emission spectrum. Our recent calculations suggest that other structures may exhibit even better thermal emission properties than the woodpile.[15] Third, we could tailor the structure to couple surface modes from the emitter into a photocell placed in close proximity. Such an approach could potentially increase the power density above the blackbody limit.[33] Now that more flexible experimental tools such as DLW are available for fabrication of metallic photonic crystals, these issues and the potential impact of these structures in energy-related applications can be more fully explored.

Acknowledgment. This work was supported by the U.S. Department of Energy under Award Number DE-FG02-06ER46438 and utilized resources at the University of Minnesota Characterization Facility, funded by NSF through the NNIN program, and the University of Minnesota Supercomputing Institute. S.E.H. and D.J.N. benefited from financial support from the Samsung and the Alexander von Humboldt Foundations, respectively. The authors thank J. Sedgewick and J. Oja for microscopy assistance.

Supporting Information Available: Experimental methods and additional figures that support the characterization of the reported materials. This material is available free of charge via the Internet at http://pubs.acs.org.

References

(1) Green, M. A., *Third Generation Photovoltaics;* Springer-Verlag: Berlin, 2003.
(2) Nozik, A. J. *Phys. E* **2002**, *14*, 115.
(3) Schaller, R. D.; Klimov, V. I. *Phys. Rev. Lett.* **2004**, *92*, 186601.
(4) Davies, P. A.; Luque, A. *Sol. Energy Mater. Sol. Cells* **1994**, *33*, 11.
(5) Coutts, T. J.; Fitzgerald, M. C. *Sci. Am.* **1998**, *279*, 90.
(6) Basu, S.; Chen, Y.-B.; Zhang, Z. M. *Int. J. Energy Res* **2007**, *31*, 689.
(7) Joannopoulos, J. D.; Villeneuve, P. R.; Fan, S. *Nature* **1997**, *386*, 143.
(8) Lin, S. Y.; Moreno, J.; Fleming, J. G. *Appl. Phys. Lett.* **2003**, *83*, 380.
(9) Cornelius, C. M.; Dowling, J. P. *Phys. Rev. A* **1999**, *59*, 4736.
(10) Fleming, J. G.; Lin, S. Y.; El-Kady, I.; Biswas, R.; Ho, K. M. *Nature* **2002**, *417*, 52.
(11) Lin, S. Y.; Fleming, J. G.; Li, Z. Y.; El-Kady, I.; Biswas, R.; Ho, K. M. *J. Opt. Soc. Am. B* **2003**, *20*, 1538.
(12) von Freymann, G.; John, S.; Schulz-Dobrick, M.; Vekris, E.; Tetreault, N.; Wong, S.; Kitaev, V.; Ozin, G. A. *Appl. Phys. Lett.* **2004**, *84*, 224.
(13) Yu, X. D.; Lee, Y. J.; Furstenberg, R.; White, J. O.; Braun, P. V. *Adv. Mater.* **2007**, *19*, 1689.
(14) Lee, J. H.; Kim, Y. S.; Constant, K.; Ho, K. M. *Adv. Mater.* **2007**, *19*, 791.
(15) Han, S. E.; Stein, A.; Norris, D. J. *Phys. Rev. Lett.* **2007**, *99*, 053906.
(16) Walsh, T. A.; Lin, S. Y. *IEEE Trans. Electron Devices* **2008**, *55*, 1101.
(17) Denny, N. R.; Han, S. E.; Norris, D. J.; Stein, A. *Chem. Mater.* **2007**, *19*, 4563.
(18) Sun, H. B.; Matsuo, S.; Misawa, H. *Appl. Phys. Lett.* **1999**, *74*, 786.
(19) Cumpston, B. H.; Ananthavel, S. P.; Barlow, S.; Dyer, D. L.; Ehrlich, J. E.; Erskine, L. L.; Heikal, A. A.; Kuebler, S. M.; Lee, I.-Y. S.; McCord-Maughon, D.; Qin, J.; Röckel, H.; Rumi, M.; Wu, X.-L.; Marder, S. R.; Perry, J. W. *Nature* **1999**, *398*, 51.
(20) Straub, M.; Gu, M. *Opt. Lett.* **2002**, *27*, 1824.
(21) Deubel, M.; von Freymann, G.; Wegener, M.; Pereira, S.; Busch, K.; Soukoulis, C. M. *Nat. Mater.* **2004**, *3*, 444.
(22) Seet, K. K.; Mizeikis, V.; Matsuo, S.; Juodkazis, S.; Misawa, H. *Adv. Mater.* **2005**, *17*, 541.
(23) Tétreault, N.; von Freymann, G.; Deubel, M.; Hermatschweiler, M.; Pérez-Willard, F.; John, S.; Wegener, M.; Ozin, G. A. *Adv. Mater.* **2006**, *18*, 457.
(24) Mizeikis, V.; Juodkazis, S.; Tarozaite, R.; Juodkazyte, J.; Juodkazis, K.; Misawa, H. *Opt. Exp.* **2007**, *15*, 8454.
(25) Tal, A.; Chen, Y. S.; Williams, H. E.; Rumpf, R. C.; Kuebler, S. M. *Opt. Exp.* **2007**, *15*, 18283.
(26) Jun, Y.; Leatherdale, C. A.; Norris, D. J. *Adv. Mater.* **2005**, *17*, 1908.
(27) Jun, Y.; Nagpal, P.; Norris, D. J. *Adv. Mater.* **2008**, *20*, 606.
(28) Mauk, M. G.; Andreev, V. M. *Semicond. Sci. Technol.* **2003**, *18*, S191.
(29) Shellenbarger, Z. A.; Taylor, G. C.; Martinelli, R. U.; Carpinelli, J. M. High performance InGaAsSb TPV cells In *Thermophotovoltaic Generation of Electricity, Sixth Conference*; Gopinath, A., Coutts, T. J., Luther, J., Eds.; American Institute of Physics: Freiburg, Germany, 2004.
(30) Kaplan, L. H.; d'Heurle, F. M. *J. Electrochem. Soc.* **1970**, *117*, 693.
(31) Vlasov, Y. A.; Bo, X. Z.; Sturm, J. C.; Norris, D. J. *Nature* **2001**, *414*, 289.
(32) Bell, P. M.; Pendry, J. B.; Martin-Moreno, L.; Ward, A. J. *Comput. Phys. Commun.* **1995**, *85*, 306.
(33) Narayanaswamy, A.; Chen, G. *Appl. Phys. Lett.* **2003**, *82*, 3544.

NL801571Z